AFRL-VS-HA-TR-2004-1202

HIGH ALTITUDE CHEMICAL INJECTIONS: NON-THERMAL CHEMICAL DYNAMICS AND FLOW FIELD MODELING

Lawrence Bernstein
Matthew Braunstein

Spectral Sciences, Inc.
4 Fourth Avenue
Burlington, MA 01803

November 2004

Scientific Report No. 4

AIR FORCE RESEARCH LABORATORY
Space Vehicles Directorate
29 Randolph Road
AIR FORCE MATERIEL COMMAND
HANSCOM AFB, MA 01731-3010

This technical report has been reviewed and is approved for publication.

RAINER DRESSLER
Contract Manager

ROBERT MORRIS, Chief
Space Weather Center of Excellence

This report has been reviewed by the ESC Public Affairs Office (PA) and is releasable to the National Technical Information Service (NTIS).

Qualified requestors may obtain additional copies from the Defense Technical Information Center (DTIC). All others should apply to the National Technical Information Service.

If your address has changed, if you wish to be removed from the mailing list, or if the addressee is no longer employed by your organization, please notify AFRL/VSIM, 29 Randolph Rd., Hanscom AFB, MA 01731-3010. This will assist us in maintaining a current mailing list.

Do not return copies of this report unless contractual obligations or notices on a specific document require that it be returned.

REPORT DOCUMENTATION PAGE

Form Approved
OMB No. 0704-0188

1. REPORT DATE *(DD-MM-YYYY)*	2. REPORT TYPE	3. DATES COVERED *(From - To)*
10-11-2004	Scientific Report No. 4	11/10/03 through 11/10/04

4. TITLE AND SUBTITLE

High Altitude Chemical Injections: Non-Thermal Chemical Dynamics and Flow Field Modeling

5a. CONTRACT NUMBER
F19628-00-C-0006

5b. GRANT NUMBER

5c. PROGRAM ELEMENT NUMBER

6. AUTHOR(S)

Lawrence Bernstein and Matthew Braunstein

5d. PROJECT NUMBER
1010

5e. TASK NUMBER
RS

5f. WORK UNIT NUMBER
A1

7. PERFORMING ORGANIZATION NAME(S) AND ADDRESS(ES)

Spectral Sciences, Inc
4 Fourth Avenue
Burlington, MA 01803-3304

8. PERFORMING ORGANIZATION REPORT NUMBER

SSI-SR-237

9. SPONSORING / MONITORING AGENCY NAME(S) AND ADDRESS(ES)

Air Force Research Laboratory
29 Randolph Road
Hanscom AFB, MA 01731-3010

10. SPONSOR/MONITOR'S ACRONYM(S)

11. SPONSOR/MONITOR'S REPORT NUMBER(S)

AFRL-VS-HA-TR-2004-1202

12. DISTRIBUTION / AVAILABILITY STATEMENT

Approved For Public Release; Distribution Unlimited

13. SUPPLEMENTARY NOTES

Near UV OH(A→X) and NH(A→X) emission bands at ~3100 and 3360 Å, respectively, have been observed in Space Shuttle engine exhaust using the GLO imager spectrograph located in the payload bay. Spectra were collected at a resolution of 4 Å for day time solar illumination conditions during low-Earth orbit (LEO) maneuvers. While it is now understood that the OH(A-X) emissions stem from solar-induced fluorescence and photodissociation of OH and H2O in the exhaust (only day phenomenon), respectively, and exhaust H2O collisions with atmospheric atomic oxygen (night and day), the NH(A-X) emissions have been determined to have a chemical reaction origin, whereby the reactants are not well established. The NH(A-X) band is of particular interest since it radiates in a spectral region where it can be readily observed from the Maui Space Surveillance Site (MSSS). In this analysis, we obtain additional clues with respect to the radiance mechanism by analyzing the temporal variation of the near-UV spectral bands.

We discuss here spectral and temporal modeling of GLO measurements of a sequence of near-UV spectra (2 s temporal resolution) recorded during an extended daytime firing of a Shuttle vernier reaction control system (VRCS) engine. In the VRCS engine burn, the spectrum is dominated by the narrow NH(A-X) band. The weaker OH(A-X) band appears to be primarily produced by the reaction of atmospheric O with exhaust H2O. This is in contrast to our analysis presented at last year's AMOS conference in which the OH emission for a higher-altitude PRCS daytime burn was dominated by solar excitation channels. As discussed here, the relative importance of the solar and reactive pathways is very sensitive to both engine thrust and altitude/atmospheric O density. We also present SOCRATES flow field and chemistry calculations of the NH(A-X) and OH(A-X) emissions. The results for both are consistent with a one-step reaction of atmospheric O with an engine-exhaust precursor.

15. SUBJECT TERMS
OH, Spectra, Shuttle, Plume, Emission, SOCRATES, DSMC, Chemistry

16. SECURITY CLASSIFICATION OF:			17. LIMITATION OF ABSTRACT	18. NUMBER OF PAGES	19a. NAME OF RESPONSIBLE PERSON
a. REPORT	b. ABSTRACT	c. THIS PAGE			R. Dressler
UNCLASSIFIED	UNCLASSIFIED	UNCLASSIFIED	SAR	19	19b. TELEPHONE NUMBER *(include area code)* (781) 377-2332

CONTENTS

FIGURES

Figure **Page**

ACKNOWLEDGEMENTS

This work has been initiated and partially funded by AFOSR under tasks 2301HS 02VS06 (program manager: Kent Miller). Some of us have been supported by the Common High Performance Computer Software Support Initiative (CHSSI) High Performance Computer Modernization Office. The authors are appreciative of key technical contributions from Rainer Dressler, Yu-hui Chiu, John Wise, James Gardner, and Edmond Murad from AFRL Space Vehicles Directorate, Hanscom, AFB also Lyle Broadfoot from the University of Arizona, Lunar and Planetary Laboratory, and Paul Sydney from the Boeing Corporation. The authors are grateful to William Dimpfl of the Aerospace, Corp. for helpful comments and contributions. The authors also gratefully acknowledge support from the Air Force Office of Scientific Research under task 2303ES02 and contract F49620-01-0095 (Program Manager: Michael R. Berman).

TEMPORAL DEPENDENCE OF THE SPECTRAL CONTENT OF LEO SPACECRAFT ENGINE-EXHAUST ATMOSPHERE INTERACTIONS

1. INTRODUCTION

Over the years, significant advances have been made in laboratory experimental techniques to study the gas-phase dynamics of chemical reaction systems in ever increasing detail. However, there remain systems that are difficult to capture in a laboratory because experimental approaches either lack the necessary sensitivity due to low number densities and small observation volumes, or do not provide the necessary control of reactant energies and densities. Remote passive optical observations of natural and man-made space-based environments have the advantage of overcoming the shortage of emitting species in a laboratory. In instances where the coupled chemical processes are well characterized, they can provide a more direct and sensitive measure of both the chemical rate coefficient and the emission spectra from the product species.

As demonstrated recently,[1-5] molecular beams emitted from a low-Earth orbit (LEO) spacecraft engine, such as a Space Shuttle Primary Reaction Control System (PRCS) engine, offer an attractive means to observe luminescent processes that follow from the hyperthermal interaction between the beam species and the ambient atmosphere. At typical LEO altitudes (200 – 400 km), the thermosphere consists of ~70 percent of atomic oxygen and ~25 percent N_2. Because the spacecraft orbit velocity is approximately 7.8 km s^{-1}, an oxygen atom penetrates the spacecraft environment with a "laboratory energy" approaching 5 eV, depending on the orbit inclination and the atmospheric co-rotational speed. This results in an average center-of-mass collision energy exceeding 2.3 eV for collisions with H_2O, a primary species of a contaminant cloud that engulfs the orbiter. Water is also a major species in the exhaust emanating from the spacecraft maneuvering engines. The flow from these engines has the characteristics of a supersonic jet with free-flow velocities exceeding 3×10^3 m s^{-1}, thereby adding additional kinetic energy to collisions with atmospheric constituents. Consequently, experiments conducted from a LEO platform can be exploited to investigate the dynamics at hyperthermal translational energies that are difficult to create in a laboratory. Knowledge of the precise orbital conditions and optical interference sources then permit the extraction of rate coefficients for luminescence processes.

During the 1990s, a suite of imagers and spectrographs called GLO was successfully flown on 5 different missions in the Space Shuttle bay providing a wealth of optical data of the Space Shuttle and near-Earth optical environment covering an unprecedented spectral range, 1150Å to 9000Å, at resolutions ranging from ~4 Å (UV) to ~10 Å (IR).[6,7] Previous analyses of this data have focused on two prominent emissions, the OH(A→X) system centered around 3086 Å and the NH(A→X) system centered around 3360 Å.[2,3] The OH(A) emissions have been determined to arise from three distinct mechanisms,

$$O\,(^3P) + H_2O \rightarrow OH\,(A^2\Sigma^+) + OH\,(X^2\Pi) \quad \Delta H = -4.79\ \text{eV}, \qquad \textbf{(R1)}$$

$$H_2O + h\nu \rightarrow OH(A) + H, \quad \text{and} \qquad \textbf{(R2)}$$

$$OH + h\nu \rightarrow OH(A). \qquad \textbf{(R3)}$$

We note that the threshold energy for reaction R1 exceeds the chemical energy available from the kinetic energy of the oxygen atoms alone. This channel is opened only when the

exhaust jet of the engine is directed into the atmospheric wind (i.e., a ram firing), where the exhaust H_2O velocity provides additional translational energy to the collision system. The rate coefficient for this chemiluminescent process has not been previously measured in the laboratory, nor has it been calculated. Recent analysis of a Shuttle PRCS ram burn has resulted in an estimated cross section of 1.7×10^{-18} cm^2;[3] the analysis reported here provides an opportunity to verify and refine this estimate. The solar UV-driven processes R2 and R3 can be expected to be prominent in day-lit conditions. Process R2 however, must also be considered in the night sky, where there is still significant VUV radiation from resonant atomic scattering from Earth's geocorona, especially when the Sun is not far below the horizon. A primary contributor of process R2 is H Lyman-a radiation at 1216 Å that provides sufficient energy to produce OH(A) with significant rotational and vibrational excitation.[8-10] There is a substantial concentration of OH (X) present in the exhaust of space engines due to the high temperatures and *kinetically-controlled* conditions within the engines.[11-13] Depending on the type of engine, the mole fraction may reach values as high as 4×10^{-3}. In contrast, *equilibrium* estimates of the exhaust OH(X) mole fraction are insignificant, $<10^{-6}$. Direct solar excitation of OH in the engine exhaust (reaction R3) is expected to produce rotationally cold OH (A) emission due to the rapid and extreme cooling resulting from supersonic vacuum expansions.

The NH(A) emissions are attributed to a single collision reaction of an engine exhaust precursor "P" with atmospheric atomic oxygen O,

$$O(^3P) + P \rightarrow NH(A) + P'O. \qquad \textbf{(R4)}$$

The identity of P is not well established, with the leading candidates being CH_2NH, HNCO, HCN, and HNC.[2] Neither are the cross section for R4 or the precursor mole fraction for a particular engine (very different mole fractions are evident for the PRCS vs VRCS engines). There is no significant solar-driven component to the NH(A) emissions as nearly the same signal level is observed for night and day firings of the same engine under comparable conditions (i.e., firing geometry and atmospheric density). This work provides an opportunity to place better bounds on the precursor mole fraction and the cross sections.

We have modeled GLO measurements of a sequence of near UV spectra (2 s temporal resolution) recorded during an extended daytime firing, ~35 s, of a Shuttle VRCS engine. In the VRCS engine burn, the spectrum is dominated by the narrow NH(A-X) band. The weaker OH(A-X) band appears to be primarily produced by the reaction of atmospheric O with exhaust H_2O. This is in contrast to our analysis presented at last year's AMOS conference in which the OH emission for a higher-altitude PRCS daytime burn was dominated by solar excitation channels.3] As discussed here, the relative importance of the solar and reactive pathways is very sensitive to altitude/atmospheric O density.

We also present SOCRATES [14] flow field and chemistry calculations of the NH(A-X) and OH(A-X) emissions. The results for both are consistent with a one-step reaction of atmospheric atomic oxygen, O, with an engine-exhaust precursor. While the on-board spectral measurements of the NH emissions provided valuable information in regard to the origin of the emissions, they offer a somewhat limited picture as they are only a single line-of-sight view through a complex 3D reactive flow field. An off-board, full spatial-spectral view of the plume, as can be observed from MSSS, recorded for different angles of attack would be invaluable in fully understanding the origin of the NH and other emissions.

2. OVERVIEW OF THE MEASUREMENTS

2.1 Low-Earth Orbit and Space Experimental Conditions

The data presented in this work were acquired from the GLO-IV spectrometer aboard the STS-74 Space Shuttle mission, which occurred between November 12 and 20, 1995. The orbital velocity is 7.7×10^3 m s^{-1}. Assuming co-rotation of the thermosphere, the spacecraft velocity with respect to the atmosphere averages ~ 7.4×10^3 m s^{-1} in the mission's West-East orbit.

In this paper we analyze the optical signals generated by a ram-fired 25 lbf thrust VRCS engine that uses N_2O_4-monomethylhydrazine (MMH) fuel. The analysis focuses on the R5R engine which was fired more or less continuously for ~35s with the detailed time history presented in Figure 1. The exhaust product mole fractions of the major species based on non-equilibrium calculations are 0.34 (H_2O), 0.31 (N_2), 0.17 (H_2), 0.14 (CO), and 0.04 (CO_2). An axial exhaust velocity of 3.5×10^3 m s^{-1} was assumed, which originates from the exit velocity of 3×10^3 m s^{-1} plus an additional 0.5×10^3 m s^{-1} attained in the vacuum expansion.[12] Thus, the overall plume-atmosphere collision velocity along the thrust axis is ~10.9×10^3 m s^{-1}, providing more than sufficient energy to enable a host of plume-atmosphere reactions giving rise to optical emissions. The firing occurred on November 18 at an altitude of 344.5 km, at 17.92 Universal Time, at -11.5 deg Latitude, and -33.3 deg Longitude. The local atmospheric conditions are a temperature of 870 K, and O and N_2 densities of 1.8×10^8 and 1.7×10^7 cm^{-3}, respectively. The thermosphere parameters associated with this measurement were retrieved from the MSIS thermosphere model.[14-16] The GLO line-of-sight (LOS) is also shown in Figure 1 and is nearly parallel to the thrust axis. At this viewing geometry, the LOS intersects the thrust axis at a distance of >50m from the nozzle exit, thereby avoiding emissions from the hot nozzle area of the exhaust while observing substantial column densities of the exhaust-atmosphere interaction region.

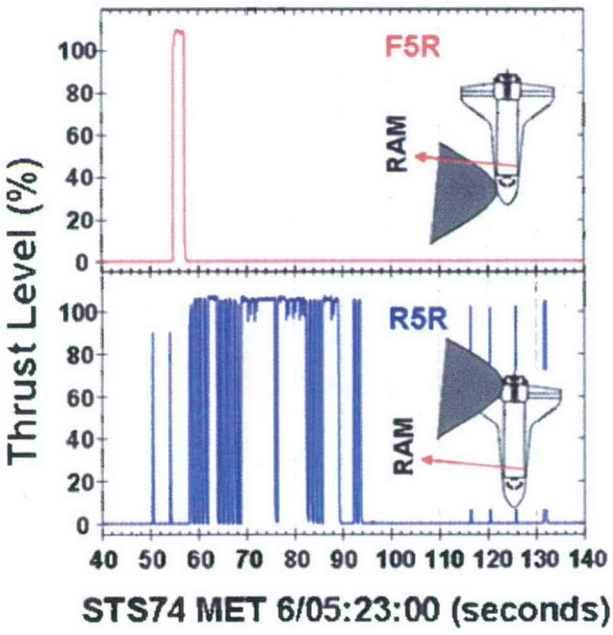

Figure 1. Firing Sequence for the R5R VRCS Engine and Measurement Geometry for the GLO Sensor. While somewhat difficult to resolve in this plot, the regions appearing as mostly solid blue actually correspond to 50 percent duty cycle pulsed engine operation with 1s on/off cycles.

2.2 The GLO Instrument and STS-74 Data

The space-borne GLO instrument has been described in detail before and was placed in the rear section of the shuttle bay during the STS-74 mission.[6,7] It comprises a nine-section spectrograph, three monochromatic imagers, and a TV camera, all boresighted to view in the same direction. The spectrograph and imagers have intensified-CCD (ICCD) focal-plane detectors. The nine slightly overlapping spectrograph sections permit simultaneous recording of the spectrum from 115.0 to 900.0 nm with a spectral resolution of about 4 to 10 Å. Their combined focal-plane image is 4500 pixels wide in the wavelength (dispersion) dimension, perpendicular to the slit, and 192 pixels in the spatial dimension, along the slit. The slit image at the detector is a narrow portion of the image of the distant object being observed, preserving spatial resolution in the slit-length direction. The design of slit and foreoptics affords a field of view of 0.2×8.5°. The spectrograph was designed to record simultaneously as much information as possible from a single column of gas, with a spectral resolution good enough to determine the intensity and the rovibrational structure of molecular emissions.

The instrument head is mounted on a scan platform that can rotate the field of view in two orthogonal directions (azimuth and elevation), thereby permitting viewing in almost any direction. The TV-camera image is used while in flight to select the view direction, track the day or night earth limb, and hold stars steady in the spectrograph slit for spectral calibrations and occultation experiments. A computer is dedicated to carrying out preprogrammed, complex experiment sequences that are time-tagged, and/or ground-commanded. The instrument is therefore autonomous and capable of continuous operation throughout a 14-day mission. Science and engineering data are returned on communications links via the TDRS satellites at a total data-return rate of 1.5 Mbits/s. A rewriteable 512-megabyte optical disk records during loss of signal on the TDRS link. Data acquisition and downloading are described in separate publications.[2,18]

The data collected in the 3000-3500 Å spectral region for the VRCS firing are shown in Figure 2. The temporal histories of the spectrally-integrated emissions are presented in Figure 3. The nearly identical temporal profiles for both emitters indicate that they both arise from chemical pathways involving the same number of reaction steps (in this case a single step reaction of a plume species with atmospheric O).

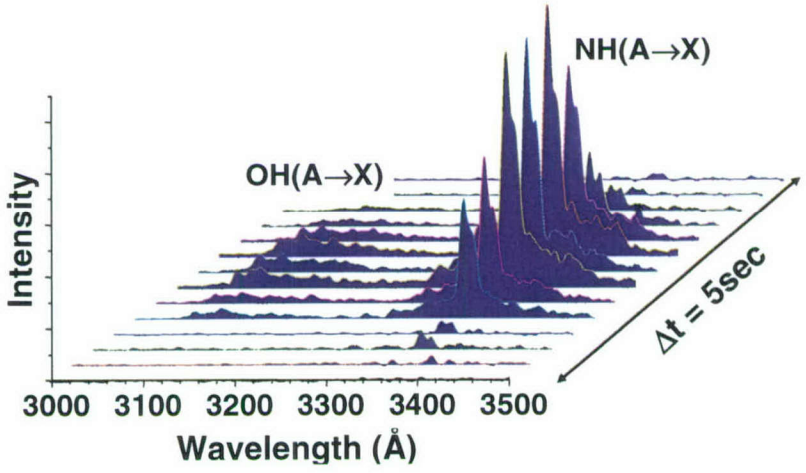

Figure 2. GLO Measurements for the OH(A-X) and NH(A-X) Spectral Emissions. The spectra were collected at 5 s intervals with 2 s averaging.

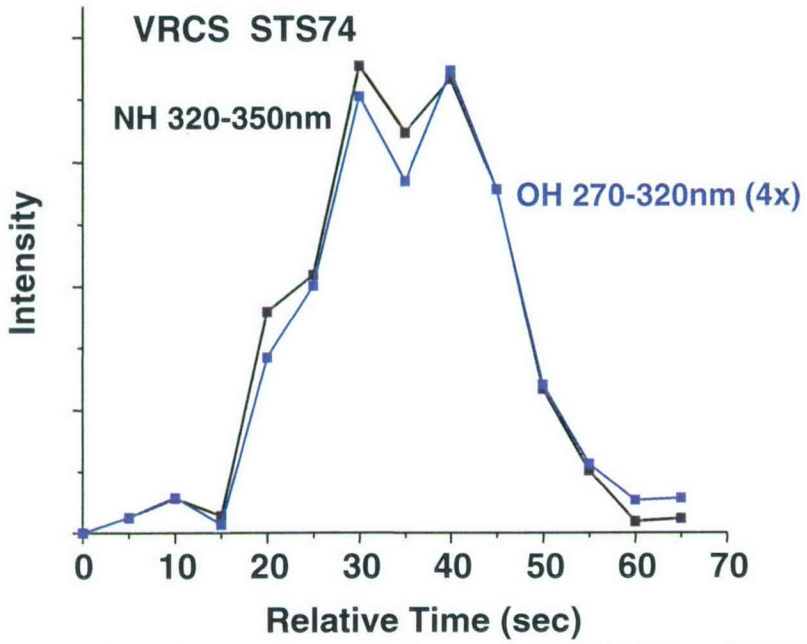

Figure 3. Temporal Profiles for the Spectrally-integrated NH(A-X) and OH(A-X) Emissions. The actual measurement times are indicated by the squares. The start of the R5R firing sequence corresponds to ~15 s on this plot.

3. DATA ANALYSIS

The OH(A) and NH(A) emission spectra are highly non-equilibrium (i.e., not simply described in terms of a single temperature). The methods and codes used to fit these spectra have been previously described.[3,4] The results are shown in Figures 4 and 5 for NH(A) and OH(A), respectively. The NH(A) fit is nearly identical to that found previously for a PRCS ram burn, indicating an identical precursor.[2] This is not surprising, as both the VRCS and PRCS engines operate with nearly identical mixture ratios of MMH/N_2O_4 and would be expected to produce the same, as yet not precisely identified, precursor. The OH(A) fit is similar to that previously determined for a PRCS night ram burn. The previous fit favored a lower rotational temperature, 4,000K, and a higher proportion of $\Delta v=1$ (region below 3000Å) emission. However, the PRCS measurement had significantly lower signal levels owing to the higher altitude, and consequently, the current fit is regarded to be more representative of the reaction-driven emission spectrum. It is noted, that even though the VRCS observation was made during the day, the contribution of the solar UV driven pathways (photo-dissociation of H_2O and solar-pumped OH fluorescence) are minor. Only the cold vacuum core OH component is seen and it accounts for ~9 percent or 8.5kR of the integrated observed intensity. This is consistent with previously described model calculations [3] of the solar components which for the VRCS engine and observation geometry (GLO sensor at far end of the payload bay) predicts 7.3kR for the OH solar-excited emission and 0.5 kR for the photo-dissociated H_2O channel. The solar-driven components scale in direct proportion to column density/vehicle thrust, whereas the reactive pathway for OH(A) is limited by the atmospheric O flux, which increases with decreasing altitude. Thus, there will be a thrust-dependent altitude below which the reactive pathway overtakes the solar UV pathways.

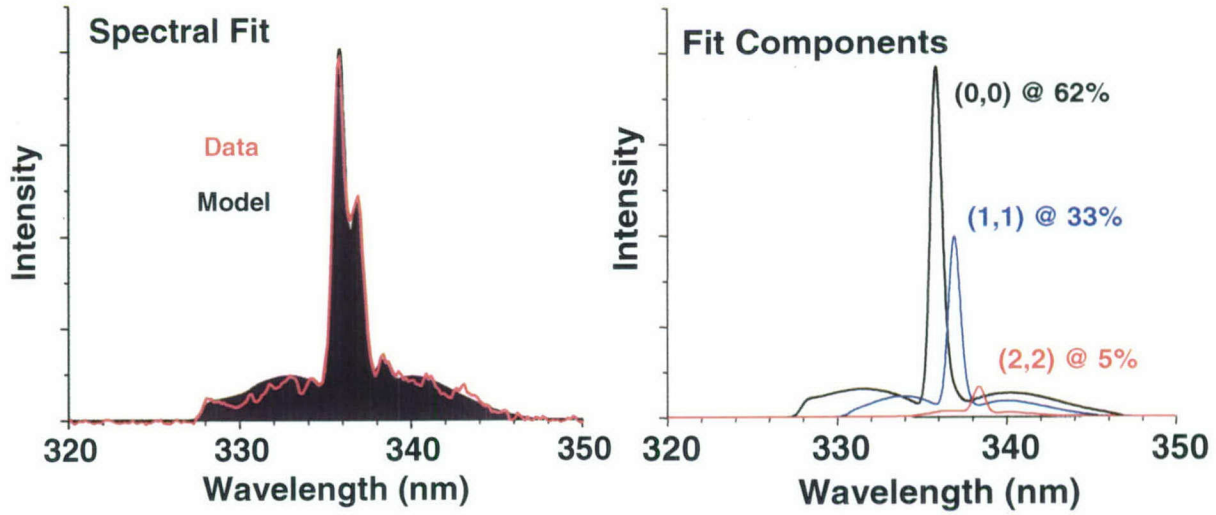

Figure 4. Spectral Fit to the NH(A-X) VRCS Data (left panel) Showing the Individual Vibrational Band Contributions (right panel). Each band required a separate rotational temperature; these are 5500, 3000, and 1000 K for the (0,0), (1,1), and (2,2) bands, respectively.

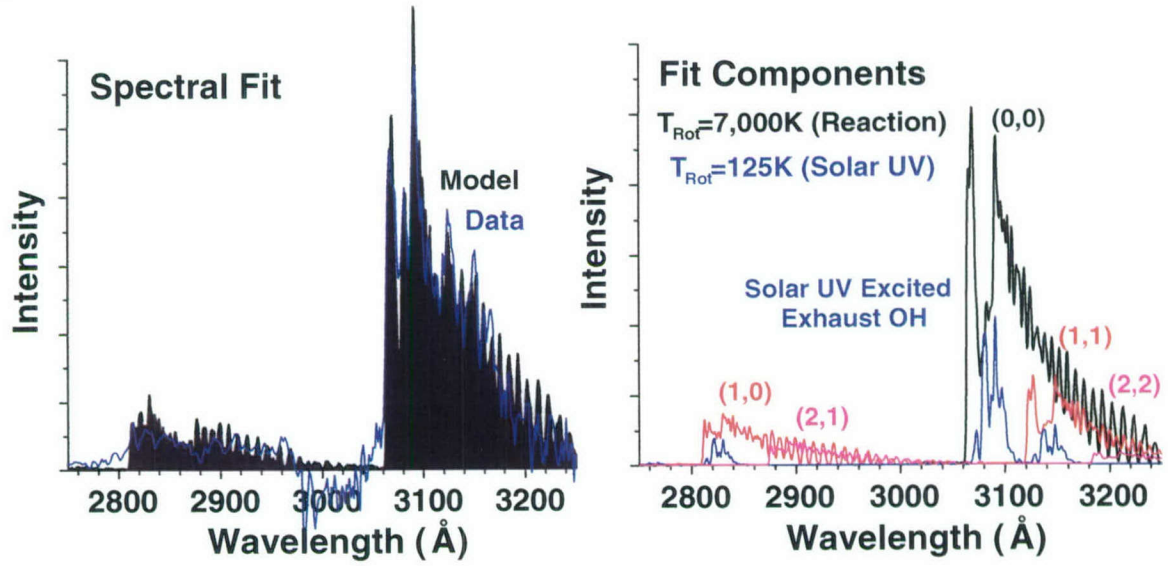

Figure 5. Spectral Fit to the OH(A-X) Data (left panel) Showing the Vibrational Band Components for the Reaction and Solar UV Excited Pathways (right panel). The fits were constrained such that the maximum allowed vibration-rotation energy for a given OH(A) state was less than the pre-dissociation threshold, E_{max}=1.5eV.

As shown recently in an analysis of the UV CO Cameron emission observed from various firings of the Shuttle OMS and PRCS engines,[3] the number of chemical steps involved in a particular emission can be inferred from the start-up or shut-down transients of the engine firing. It was found that a simple, approximate chemical kinetic approach yielded results (i.e., the temporal intensity profile) comparable to more accurate and detailed Direct Simulation Monte Carlo (DSMC) based calculations using the SOCRATES code.[14] For an arbitrary engine firing sequence, the intensity (both the LOS and total spatial emission) for a one-step mechanism can be approximated by

$$I(t') = I_o \int_0^{t'} dt F(t) \exp(-(t'-t)/t_1), \quad (1)$$

where F(t) is the thrust level, I_o is a normalization constant, and t_1 is the single-collision time constant for an exhaust species with the atmospheric O. The collision time constant is estimated from

$$t_1 = \frac{1}{\rho \sigma u}, \quad (2)$$

where ρ is the total ambient density, σ is the elastic scattering cross section, and u is the relative collision velocity. We evaluated Eq.(1) for the VRCS firing sequence of Figure 1 using $\rho=2.0\times10^{8}$ cm^{-3}, $\sigma=1.1\times10^{-15}$ cm^2 (estimated for O-NH precursor collisions), and $u=10.9\times10^{5}$ cm s^{-1}. The time constant is $t_1=3.8$ s, which represents an effective rise or decay time for engine start-up or shutdown. The comparison of the predicted temporal emission profile to that observed for the NH(A) (the OH(A) is virtually identical - see Figure 1) is depicted in Figure 6. The overall agreement is good and further confirms that both the VRCS NH(A) and OH(A) emissions are formed by one-step reactions.

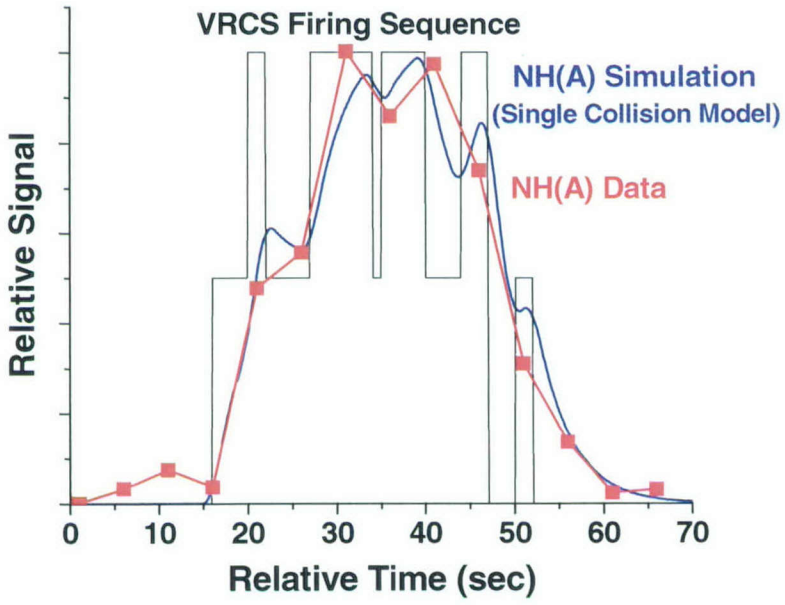

Figure 6. Comparison of the Modeled Intensity Profile for the NH(A) Emission Based on a Single-collision Kinetic Model to the Observation (the squares correspond to the measurement times). For simplicity, a slightly temporally-averaged representation of the actual firing sequence (see Figure 1) was employed. A 2 s box-car average was applied to the model profile to simulate the GLO sensor temporal integration.

Predictions of the NH(A) and OH(A) emissions were performed using the SOCRATES high-altitude chemistry, flow field, and radiation code. The velocity-dependent cross sections for the single-step chemistries used in the calculations are displayed in Figure 7. The OH(A) cross sections were recently deduced from analysis of a Shuttle PRCS night ram burn.[3] It is noted that this chemistry turns on steeply near the ram firing collision velocity of 10.9 km s^{-1}. It is seen that the distribution of collision velocities due to the thermal spread in O atom velocities plays an

important part in enhancing the effective reaction cross section, as it accesses the much larger higher-velocity portion of the cross section curve. The NH(A) cross sections are based on earlier analyses,[2] however these studies did not establish the absolute value of this curve. For the SOCRATES NH(A) calculations, a precursor exhaust mole fraction of 0.001 was adopted; however, we are using the comparison to the observed absolute intensity as a guide in recommending improved values for both the cross sections and precursor concentration estimates. The results are shown in Figure 8 for both the on-board observation geometry and for a remote observer as would be the case for viewing Shuttle firings from MSSS. The OH(A) prediction of ~110 kR agrees well with the observed value of 85 kR, and demonstrates that the previously-derived cross section applies satisfactorily to a much lower-altitude higher-density and lower thrust observation. However, the NH(A) prediction of ~4.7 kR is a factor of 80 lower than the observed peak/steady-state intensity of 377 kR. This necessitates that the product of the cross section and precursor concentration be increased by the same factor. The cross section at 10.9 km s^{-1} is 40 times below the gas kinetic limit and the assumed precursor mole fraction of 0.001 has up to about a factor of 10× wiggle room. Thus, the shortfall can be easily accommodated by judicious increases in these quantities. Our current intuition favors increasing the cross section pre-exponential by a factor of 16 to 5.9×10^{-10} cm^3 s^{-1} and allowing the VRCS precursor concentration to increase to 0.005.

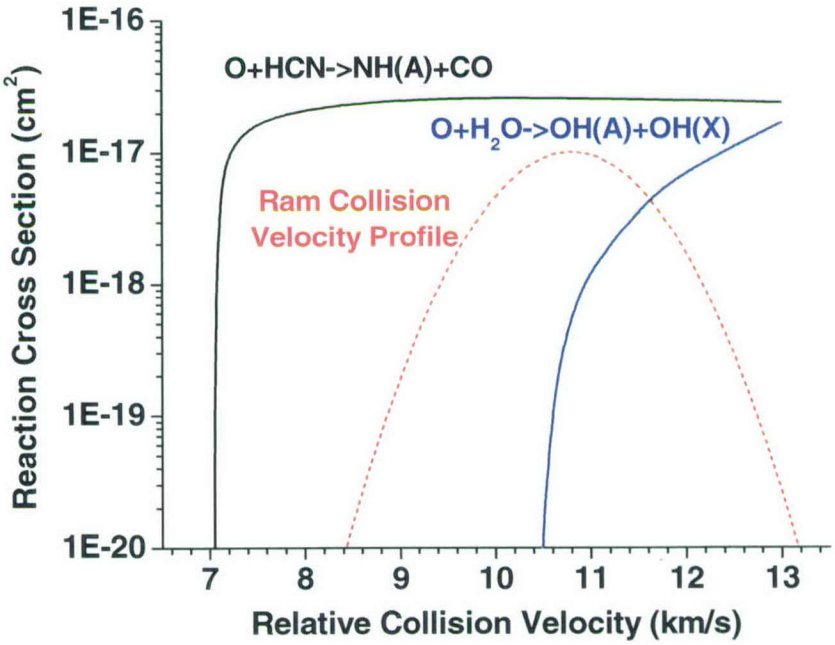

Figure 7. Velocity-dependent Cross Sections for the Rate Constants Representing the NH(A) and OH(A) Reaction Pathways. The rate constants are $3.7\times10^{-11}\exp(-56.5$ kcal/RT) and 1.0×10^{-16} $T^{1.3}\exp(-110.2$ kcal/RT) cm^3 s^{-1} for NH(A) and OH(A), respectively. The relative distribution of collision velocities about the mean ram collision velocity of 10.9 km s^{-1} and the local atmospheric temperature of 870 K is also shown.

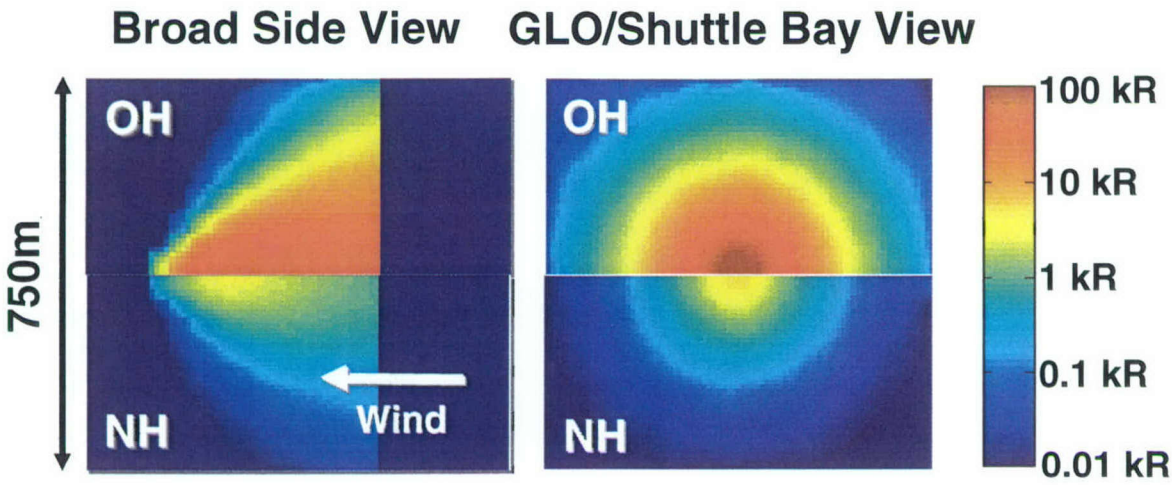

Figure 8. SOCRATES Computed Total Spectral Emissions for the NH(A) and OH(A) Bands Based on the Cross Sections Displayed in Figure 7.

4. CONCLUSIONS AND FUTURE DIRECTIONS

The major conclusions of this study are:

- The temporal evolution of the NH(A) and OH(A) emissions for STS74 are consistent with a single-step reaction of a plume species with atmospheric O.
- Relative contributions of solar UV and reaction path ways for OH(A) is highly altitude dependent
- This analysis supports and refines previous retrievals of spectral parameters and reaction cross sections for NH(A) and OH(A). We recommend a revised NH(A) formation rate constant of $5.9\times10^{-10}\exp(-56.5\ \text{kcal/RT})\ \text{cm}^3\ \text{s}^{-1}$ based on a precursor exhaust mole fraction of 0.001

Future directions include:

- Off-board spatially, spectrally, and temporally resolved observations of the *entire* interaction region would result in significantly improved spectral parameters, transport cross sections, and cross sections for key IR-UV emissions.
- MSSS-based observations of Shuttle firings are in the planning stages and are designated as the Maui Analysis of Upper-Atmospheric Injections (MAUI). We are also exploring observations of the Russian International Space Station cargo vehicle, Progress.

REFERENCES

1. Murad, E., D. J. Knecht, R. A. Viereck, C. P. Pike, I. L. Kofsky, C. A. Trowbridge, D. L. A. Rall, G. Ashley, L. Twist, J. B. Elgin, A. Setayesh, J. A. T. Stair, and J. E. Blaha, 1990, *Geophys. Res. Lett.,* **Vol. 17**, 2205.
2. Viereck, R. A., E. Murad, D. J. Knecht, C. P. Pike, L. S. Bernstein, J. B. Elgin, and A. L. Broadfoot, 1996, *J. Geophys. Res.,* **Vol. 101**, 5371.
3. Dimpfl, W. L., G. C. Light, and L. S. Bernstein, Accepted, 2004, *J. Spacecraft and Rockets.*
4. Xiaofeng, T., Diatomic: A powerful spectral simulation program for diatomic molecules on Windows platforms, release 1.28, 2004; Xiaofeng, T., Diatomic: A powerful spectral simulation program for diatomic molecules, the Ohio State University 57th International Symposium on Molecular Spectroscopy, Columbus, TA01 2002.
5. Bernstein, L. S., Chiu, Y., Gardner, J. A., Broadfoot, A. L., Lster, M. I., Tsiouris, M., Dressler, R., and Murad, E., 2003, *J. Phys. Chem.,* **Vol. 107**, 10695.
6. Broadfoot, L. A., http://glo.lpl.arizona.edu/glo.
7. Broadfoot, A. L., Sandel, B. R., Knecht, D. J., Viereck, R. A., and Murad, 1992, *E., Appl. Opt.,* **Vol. 31**, 3083.
8. Mordaunt, D. H., Ashfold, M. N. R., and Dixon, R. N., 1994, *J. Chem. Phys.,* **Vol. 199**, 7360.
9. Harich, S. A., H. Hwang, D. W., Yang, X., Lin, J. J., Yang, X., and Dixon, R. N., 2000, *J. Chem. Phys.*, **Vol. 113**, 10073.
10. Carrington, T., 1964, *J. Chem. Phys.*, **Vol. 41**, 2012.
11. Pickett, J. S., Murphy, G. R., Kurth, W. S., Goertz, C. K., and Shawhan, S. D., 1985, *J. Geophys. Res.,* **Vol. 90**, 3487.
12. Pickett, J. S., Murphy, G. B., and Kurth, W. S., 1988, *J. Spacecraft Rockets,* **Vol. 25**, 169.
13. Viereck, R. A., Bernstein, L. S., Mende, L. S., Murad, S. B., and Swenson, E., 1993 *J. Spacecraft Rockets,* **Vol. 30,** 724.
14. Cho, J., M. Braunstein, and J. B. Elgin, 1995, SOCRATES 3.0 User's Manual.
15. Hedin, A. E., 2003, The NRL Mass Spectrometer, Incoherent Scatter Radar Extended Model: NRLMSISE-00, http://uap-www.nrl.navy.mil/models_web/msis/msis_home.htm.
16. Hedin, A. E., 1991, *J. Geophys. Res.,* **Vol. 96**, 1159.
17. Hedin, A. E., 1987, *J. Geophys. Res.,* **Vol. 92**, 4649.
18. Knecht, D. J., Murad, E., Viereck, R., Pike, C. P., Broadfoot, A. L., Anderson, E. R., Hatfield, D. B., Stone, T. C., and Sandel, B. R., 1997, *Adv. Space Res.,* **Vol. 19**, 627.